Contribution from the Chemistry Department,
University of Queensland St. Lucia, QLD 4067, Australia

Role of the Trigonal $t_{2e}^{2-n}e^n$ Single-Ion Configuration in d^3d^3 Metal–Metal σ-Bonded Dimers

Robert Stranger

Received December 27, 1989

The theory of the trigonal $t_{2e}^{2-n}e^n$ single-ion and $(t_{2e}^{2-n}e^n)_a(t_{2e}^{2-n}e^n)_b$ pair configurations is presented in which account is taken of the single-ion electron repulsion, cubic and trigonal ligand fields, Zeeman splitting, and the M–M π interaction of the pair. Application of the theory to the electronic spectra of $Mo_2X_9^{3-}$ (X = Cl, Br) species offers a viable explanation for the broad spin-allowed bands observed above 16 000 cm^{-1} in terms of singly excited pair states involving the trigonal $t_{2e} \rightarrow e$ orbital transition. Furthermore, the anomalously low orbital g values reported previously for the lower lying pair multiplets in the chloro complex[1] can be explained by extensive mixing of the single-ion t_{2e} and e orbitals by the M–M π interaction and are consistent with the value of $J_\pi \approx 7000$ cm^{-1} obtained from a recent analysis of the double excitation region of the electronic spectrum of $Cs_3Mo_2Cl_9$.[2]

Introduction

In an earlier study,[1] we presented a detailed analysis of the electronic spectrum of $Cs_3Mo_2Cl_9$ below 16 000 cm^{-1} on the basis of a theoretical model involving the full $t_2^3t_2^3$ pair configuration, incorporating both the M–M σ and π exchange interactions. The cubic e_g orbitals were not included in the above model, since in the absence of M–M π bonding, the t_{2g} and e_g orbitals are not mixed by the M–M σ interaction. The conclusion reached from that study was that the M–M σ bond was quite strong with much weaker π bonding, resulting in an almost complete factoring out of pair states involving electron occupation of the trigonal t_{2z} orbital. The states converging to lower energy below 16 000 cm^{-1} were found to correspond to those predicted for an effective $t_{2e}^2t_{2e}^2$ pair configuration in which the trigonal t_{2z} orbitals are absent due to their participation in M-M σ bonding.

The $t_{2e}^2t_{2e}^2$ pair configuration comprises the $^3A_2{}^3A_2$ ground state, $^3A_2{}^1E$ and $^3A_2{}^1A_1$ singly excited and $^1E^1E$, $^1E^1A_1$, and $^1A_1{}^1A_1$ doubly excited pair states. These states are derived from the $^4A_2{}^4A_2$ ground state, $^4A_2{}^2E$ and $^4A_2{}^2T_{20}$ singly excited pair state, and $^2E^2E$, $^2E^2T_{20}$, and $^2T_{20}{}^2T_{20}$ doubly-excited $t_2^3t_2^3$ pair state, respectively, in the absence of any M–M σ bonding. Unfortunately, we were not able to unambiguously assign the $^3E'$ level of the singly excited $^3A_2{}^1E$ pair state at approximately 8000 cm^{-1}. A reliable estimate of the M–M π bonding based on this band region is therefore not possible, though initial assignments[1] had indicated J_π to be quite small, less than 1000 cm^{-1}. However, the recent analysis[2] of the $^1E^1E$ double excitation around 13 000 cm^{-1} in $Cs_3Mo_2Cl_9$ has shown that J_π is not small but is approximately 7000 cm^{-1} with $J_\sigma = 25000 \pm 5000$ cm^{-1}. Therefore, neglect of the e_g orbitals in the theoretical analysis is not justified.

Although the $t_2^3t_2^3$ pair model provides a satisfying explanation of the observed multiplet structure below 16 000 cm^{-1} in the electronic spectrum of $Cs_3Mo_2Cl_9$, it cannot account for the anomalously low orbital g values found for certain of the $t_{2e}^2t_{2e}^2$ pair states. Furthermore, there remains the problem of assigning the broad spin-allowed bands observed above 16 000 cm^{-1} in both the chloro and the bromo complexes.[3-5] In the past, due to the fortuitous resemblance to monomeric MoX_6^{3-} (X = Cl, Br) spectra,[4-6] these bands have been assigned on the basis of d^3 single-ion excitations. Clearly, since the lower energy multiplets have demonstrated the presence of strong M–M σ bonding, such assignments lack credibility.

Ideally, what is required is a complete d^3d^3 calculation involving both the t_{2g} and e_g orbitals. However, such a calculation involves an awesome pair basis size of 14 400 which is clearly impractical, and in many respects unnecessary, since it has been shown that the lower lying multiplets in the electronic spectrum of $Cs_3Mo_2Cl_9$ correspond to an effective $t_{2e}^2t_{2e}^2$ pair configuration. It is therefore useful to consider the $(t_{2e}^{2-n}e^n)_a(t_{2e}^{2-n}e^n)_b$ pair configuration which not only includes those states arising from the $t_{2e}^2t_{2e}^2$ configuration, but also those resulting from electron promotion to the cubic e_g orbitals. In this respect, the full effect of M–M π bonding on the pair states can be ascertained. The results thus obtained will be relevant to the electronic spectra of not only $Mo_2X_9^{3-}$ species but also the tungsten(III) analogues exhibiting much stronger M–M π bonding.[7,8]

Theory

(a) The $t_{2e}^{2-n}e^n$ Configuration. The trigonal $t_{2e}^{2-n}e^n$ single-ion configuration derives from the octahedral d^3 configuration when the t_{2z} orbital and its accompanying electron are factored out energetically. This may result from a large trigonal field or strong M–M σ bonding in the case of dimeric systems. This configuration comprises t_{2e}^2, $t_{2e}^1e^1$, and e^2 subconfigurations, which span a total of 12 multiplets (28 spin-orbit components) given by

$$t_{2e}^2: \ {}^3A_2 + {}^1A_1 + {}^1E$$

$$t_{2e}^1e^1: \ {}^3A_1 + {}^3A_2 + {}^3E + {}^1A_1 + {}^1A_2 + {}^1E$$

$$e^2: \ {}^3A_2 + {}^1A_1 + {}^1E$$

The wave functions corresponding to the above states can be constructed by using standard group theoretical techniques[9,10] as

$$|t_{2e}^{2-n}e^n\, S\Gamma M\gamma\rangle = \sum_{\substack{m_1m_2\\ \gamma_1\gamma_2}} (-1)^M(2S+1)^{1/2}[\lambda(\Gamma)]^{1/2} \times \begin{pmatrix} \frac{1}{2} & \frac{1}{2} & S \\ m_1 & m_2 & -M \end{pmatrix} V \begin{pmatrix} e & e & \Gamma \\ \gamma_1 & \gamma_2 & \gamma \end{pmatrix} |\tfrac{1}{2}t_{2e}\, m_1\gamma_1\rangle|\tfrac{1}{2}e\, m_2\gamma_2\rangle \quad (1)$$

where the coupling coefficient for spin angular momentum corresponds to Wigner's $3j$ coefficient[9] and the V coefficient is that of Griffith's real trigonal basis.[10] Note that t_{2e} transforms as the E representation in C_{3v} point group symmetry. The wave functions for the $|t_{2e}^2\, S\Gamma M\gamma\rangle$ and $|e^2\, S\Gamma M\gamma\rangle$ states are constructed similarly, except that the one-electron product functions will both contain either t_{2e} or e orbitals. The appropriate trigonal one-electron orbitals expressed in terms of cubic components quantized down the trigonal axis are

$$t_{2x} = (\sqrt{2}(x^2 - y^2) - xz)/\sqrt{3}$$

$$t_{2y} = -(\sqrt{2}xy + yz)/\sqrt{3}$$

$$e_x = (\sqrt{2}xz + x^2 - y^2)/\sqrt{3}$$

$$e_y = (\sqrt{2}yz - xy)/\sqrt{3} \quad (2)$$

(1) Dubicki, L.; Krausz, E.; Stranger, R.; Smith, P. W.; Tanabe, Y. *Inorg. Chem.* **1987**, *26*, 2247.
(2) Stranger, R. *Chem. Phys. Lett.* **1989**, *157*, 472.
(3) Lewis, J.; Nyholm, R. S.; Smith, P. W. *J. Chem. Soc. A* **1969**, 57.
(4) Smith, P. W.; Wedd, A. G. *J. Chem. Soc. A* **1970**, 2447.
(5) Nguen Hyu Chi; Zelentsov, V. V.; Subbotina, N. A.; Spitsyn, V. I.; Fal'kengof, A. T. *Russ. J. Inorg. Chem. (Engl. Transl.)* **1972**, *17*, 1715.
(6) Furlani, C.; Piovesana, O. *Mol. Phys.* **1965**, *9*, 341.
(7) Summerville, R. H.; Hoffmann, R. *J. Am. Chem. Soc.* **1979**, *101*, 3821.
(8) Natkaniec, L. *Bull. Acad. Pol. Sci., Ser. Sci. Chim.* **1978**, *26*, 241.
(9) Silver, B. L. *Irreducible Tensor Methods*; Academic Press: New York, 1976.
(10) Griffith, J. S. *The Irreducible Tensor Method for Molecular Symmetry Groups*; Prentice Hall: Englewood Cliffs, NJ, 1962.

0020-1669/90/1329-5231$02.50/0

Table I. Wave Functions for the $t_{2e}^{2-n}e^n$ Single-Ion Configuration[a]

t_{2e}^2	$\|^3A_2\rangle = (1/\sqrt{2})(\|t_{2x}^+t_{2y}^-\| - \|t_{2y}^+t_{2x}^-\|)$
	$\|^1A_1\rangle = (1/\sqrt{2})(\|t_{2x}^+t_{2x}^-\| + \|t_{2y}^+t_{2y}^-\|)$
	$\|^1E_x\rangle = (1/\sqrt{2})(\|t_{2y}^+t_{2y}^-\| - \|t_{2x}^+t_{2x}^-\|)$
	$\|^1E_y\rangle = (1/\sqrt{2})(\|t_{2x}^+t_{2y}^-\| + \|t_{2y}^+t_{2x}^-\|)$
$t_{2e}^1e^1$	$\|^3A_1\rangle = (1/2)(\|t_{2x}^+e_x^-\| + \|t_{2x}^-e_x^+\| + \|t_{2y}^+e_y^-\| + \|t_{2y}^-e_y^+\|)$
	$\|^3A_2\rangle = (1/2)(\|t_{2x}^+e_y^-\| + \|t_{2x}^-e_y^+\| - \|t_{2y}^+e_x^-\| - \|t_{2y}^-e_x^+\|)$
	$\|^3E_x\rangle = (1/2)(\|t_{2y}^+e_y^-\| + \|t_{2y}^-e_y^+\| - \|t_{2x}^+e_x^-\| - \|t_{2x}^-e_x^+\|)$
	$\|^3E_y\rangle = (1/2)(\|t_{2x}^+e_y^-\| + \|t_{2x}^-e_y^+\| + \|t_{2y}^+e_x^-\| + \|t_{2y}^-e_x^+\|)$
	$\|^1A_1\rangle = (1/2)(\|t_{2x}^+e_x^-\| - \|t_{2x}^-e_x^+\| + \|t_{2y}^+e_y^-\| - \|t_{2y}^-e_y^+\|)$
	$\|^1A_2\rangle = (1/2)(\|t_{2x}^+e_y^-\| - \|t_{2x}^-e_y^+\| - \|t_{2y}^+e_x^-\| + \|t_{2y}^-e_x^+\|)$
	$\|^1E_x\rangle = (1/2)(\|t_{2y}^+e_y^-\| - \|t_{2y}^-e_y^+\| - \|t_{2x}^+e_x^-\| + \|t_{2x}^-e_x^+\|)$
	$\|^1E_y\rangle = (1/2)(\|t_{2x}^+e_y^-\| - \|t_{2x}^-e_y^+\| + \|t_{2y}^+e_x^-\| - \|t_{2y}^-e_x^+\|)$
e^2	$\|^3A_2\rangle = (1/\sqrt{2})(\|e_x^+e_y^-\| - \|e_y^+e_x^-\|)$
	$\|^1A_1\rangle = (1/\sqrt{2})(\|e_x^+e_x^-\| + \|e_y^+e_y^-\|)$
	$\|^1E_x\rangle = (1/\sqrt{2})(\|e_y^+e_y^-\| - \|e_x^+e_x^-\|)$
	$\|^1E_y\rangle = (1/\sqrt{2})(\|e_x^+e_y^-\| + \|e_y^+e_x^-\|)$

[a] Only the $M = 0$ spin components given.

Table II. One-Electron Reduced Matrix Elements of the Electron Repulsion Operator[a]

$\langle t_2\|\|g_0(A_1)\|\|t_2\rangle = \sqrt{(3F_0)}$	$\langle e\|\|g_0(A_1)\|\|e\rangle = \sqrt{(2F_0)}$
$\langle t_2\|\|g_4(A_1)\|\|t_2\rangle = 2\sqrt{(7F_4)}$	$\langle e\|\|g_4(A_1)\|\|e\rangle = -\sqrt{(42F_4)}$
$\langle t_2\|\|g_2(E)\|\|t_2\rangle = 2\sqrt{(3F_2)}$	$\langle e\|\|g_2(E)\|\|e\rangle = -4\sqrt{(F_2)}$
$\langle t_2\|\|g_4(E)\|\|t_2\rangle = 4\sqrt{(5F_4)}$	$\langle e\|\|g_4(E)\|\|e\rangle = 2\sqrt{(15F_4)}$
$\langle t_2\|\|g_2(T_2)\|\|t_2\rangle = -3\sqrt{(2F_2)}$	$\langle t_2\|\|g_4(T_2)\|\|t_2\rangle = 2\sqrt{(30F_4)}$
$\langle t_2\|\|g_4(T_1)\|\|e\rangle = -\sqrt{(105F_4)}$[b]	$\langle t_2\|\|g_2(T_2)\|\|e\rangle = 2\sqrt{(3F_2)}$
$\langle t_2\|\|g_4(T_2)\|\|e\rangle = 3\sqrt{(5F_4)}$	

[a] Taken from ref 11. [b] Changes sign on interchange of t_2 and e.

By the use of expression 1, the $M = 0$ spin component of all states have been determined and are listed in Table I.

Electrostatic Interaction. As shown by Griffith,[10] the electron repulsion operator can be expressed as a product of one-electron operators in the form

$$G = \sum_{j<k} e^2/r_{jk} = \sum_{i\Gamma\gamma} \sum_{j<k} g_{i\Gamma\gamma}(j)\, g_{i\Gamma\gamma}(k) \qquad (3)$$

where j and k sum over the electrons and the $g_{i\Gamma\gamma}$ are one-electron operators transforming as the irreducible representation Γ with component γ. In the above expression, i sums over the spherical harmonics of zero-, second-, and fourth-order rank, which may form different bases for the same irreducible representation $\Gamma\gamma$. As such, the matrix elements of $g_{i\Gamma\gamma}$ are proportional to the square root of the Slater–Condon parameters F_0, F_2, and F_4 for d^n configurations. Application of the Wigner–Eckhart theorem to the matrix elements of G leads to the expression

$$\langle \Gamma_1\gamma_1\Gamma_2\gamma_2|G|\Gamma_1'\gamma_1'\Gamma_2'\gamma_2'\rangle = \sum_{i\Gamma\gamma} V\begin{pmatrix}\Gamma & \Gamma_1' & \Gamma\\ \gamma_1 & \gamma_1' & \gamma\end{pmatrix} V\begin{pmatrix}\Gamma_2 & \Gamma_2' & \Gamma\\ \gamma_2 & \gamma_2' & \gamma\end{pmatrix} \langle \Gamma_1||g_{i\Gamma\gamma}||\Gamma_1'\rangle\langle \Gamma_2||g_{i\Gamma\gamma}||\Gamma_2'\rangle \qquad (4)$$

where $\Gamma_1\gamma_1$, $\Gamma_1'\gamma_1'$ and $\Gamma_2'\gamma_2'$ label the orbitals involved, which, for the cubic group, span t_2 + e representations. For the $g_{i\Gamma}$ operators, Γ is restricted to those representations that are contained in both direct products $\Gamma_1 \times \Gamma_1'$ and $\Gamma_2 \times \Gamma_2'$. Furthermore, if $\Gamma_1 = \Gamma_1'$ or $\Gamma_2 = \Gamma_2'$, then Γ is restricted to the symmetrized squares $[\Gamma_1]^2$ or $[\Gamma_2]^2$, which span $A_1 + E + T_2$ and $A_1 + E$ representations for the t_2 and e orbitals, respectively. The necessary reduced matrix elements in (4) have been tabulated by Daul and Day[11] and are listed in Table II in terms of the F_k parameters.

For the real trigonal orbitals given above, it is necessary to use the trigonal V coefficients tabulated by Griffith[10] in evaluating the matrix elements of G. With the use of expression 4, the electrostatic integrals were calculated for the trigonally adapted

(11) Daul, C.; Day, P. *Mol. Phys.* **1977**, *33*, 1421.

Table III. Electrostatic Integrals for the Trigonal t_{2e} and e Orbitals[a]

$$J(x,x) = J(X,X) = F_0 + 4F_2 + 36F_4 = A + 4B + 3C$$
$$J(x,y) = J(x,X) = F_0 - 2F_2 - 4F_4 = A - 2B + C$$
$$J(x,Y) = F_0 + 2F_2 - 24F_4 = A + 2B + C$$
$$J(X,Y) = F_0 - 4F_2 + 6F_4 = A - 4B + C$$
$$K(x,y) = K(x,X) = 3F_2 + 20F_4 = 3B + C$$
$$K(x,Y) = F_2 + 30F_4 = B + C$$
$$K(X,Y) = 4F_2 + 15F_4 = 4B + C$$

$$\langle xX||Yy\rangle = F_2 - 5F_4 = B$$
$$\langle xX||yY\rangle = \langle xY||Xy\rangle = -2F_2 + 10F_4 = -2B$$
$$\langle xy||xY\rangle = \langle xy||Xy\rangle = 2\sqrt{2}F_2 - 10\sqrt{2}F_4 = 2\sqrt{2}B$$
$$\langle xy||Yx\rangle = \langle xy||yX\rangle = -\sqrt{2}F_2 + 5\sqrt{2}F_4 = -\sqrt{2}B$$

[a] Where x, y, and X, Y are components of the t_{2e} and e orbitals, respectively. Other integrals can be found from the interchange ($x \rightarrow y$, $y \rightarrow x$) and ($X \rightarrow Y$, $Y \rightarrow X$).

Table IV. Electrostatic Energies for the $t_{2e}^{2-n}e^n$ Single-Ion States

t_{2e}^2	$\|^3A_2\rangle = A - 5B$
	$\|^1E\rangle = A + B + 2C$
	$\|^1A_1\rangle = A + 7B + 4C$
$t_{2e}^1e^1$	$\|^3A_2\rangle = A + 4B + \Delta$
	$\|^3A_1\rangle = A - 8B + \Delta$
	$\|^3E\rangle = A - 2B + \Delta$
	$\|^1A_2\rangle = A + 4B + 2C + \Delta$
	$\|^1A_1\rangle = A + 2C + \Delta$
	$\|^1E\rangle = A + 2B + 2C + \Delta$
e^2	$\|^3A_2\rangle = A - 8B + 2\Delta$
	$\|^1E\rangle = A + 8B + 4C + 2\Delta$
	$\|^1A_1\rangle = A + 2C + 2\Delta$

$$\langle t_{2e}^2\ {}^3A_2||t_{2e}^1e^1\ {}^3A_2\rangle = 6B$$
$$\langle t_{2e}^2\ {}^1A_1||t_{2e}^1e^1\ {}^1A_1\rangle = -2B$$
$$\langle t_{2e}^2\ {}^1A_1||e^2\ {}^1A_1\rangle = 4B + 2C$$
$$\langle t_{2e}^2\ {}^1E||t_{2e}^1e^1\ {}^1E\rangle = 2B$$
$$\langle t_{2e}^2\ {}^1E||e^2\ {}^1E\rangle = 2B$$

t_{2g} and e_g orbitals. The nonzero integrals are listed in Table III in terms of both the Slate–Condon F_k and Racah A, B, and C parameters. Finally, from the two-electron wave functions and electrostatic integrals given in Tables I and III, respectively, the electrostatic energies for the multiplets arising from the trigonal $t_{2e}^{2-n}e^n$ single-ion configuration are readily calculated and are given in Table IV. In this table Δ is the energy separation of the t_{2e} and e orbitals, which, in the cubic case, corresponds to $10Dq$.

Orbital Moments. In order to predict the g values for the $(t_{2e}^{2-n}e^n)_a(t_{2e}^{2-n}e^n)_b$ pair states, the single-ion orbital moments must be calculated. From the one-electron orbital moments

$$\langle t_{2x}|l_z|t_{2y}\rangle = ik \qquad \langle t_{2x}|l_z|e_y\rangle = i\sqrt{2}k' \qquad (5)$$

where the orbital components x and y refer to the trigonal quantization and k and k' are the one-electron orbital reduction parameters, the orbital moments for the $t_{2e}^{2-n}e^n$ single-ion multiplets can be calculated by using the wave functions given in Table I. The nonzero matrix elements are found to be

$$\langle t_{2e}^2\ {}^1e_x|L_z|t_{2e}^2\ {}^1E_y\rangle = -i\,2k$$
$$\langle t_{2e}^1e^1\ {}^3E_x|L_z|t_{2e}^1e^1\ {}^3E_y\rangle = -ik$$
$$\langle t_{2e}^1e^1\ {}^1E_x|L_z|t_{2e}^1e^1\ {}^1E_y\rangle = -ik$$
$$\langle t_{2e}^2\ {}^1E_x|L_z|t_{2e}^1e^1\ {}^1E_y\rangle = -i\,2k'$$
$$\langle t_{2e}^1e^1\ {}^1E_x|L_z|e^2\ {}^1E_y\rangle = -i\,2k' \qquad (6)$$

(b) The $(t_{2e}^{2-n}e^n)_a(t_{2e}^{2-n}e^n)_b$ Pair Configuration. From the 28 $t_{2e}^{2-n}e^n$ single-ion spin–orbit states, a total of 784 pair spin–orbit states occur. However, if spin–orbit coupling is ignored, the pair basis size reduces to 328, corresponding to the $M = 0$ spin components only. This basis breaks up into 136 ($S = 0$), 156 ($S = 1$), and 36 ($S = 2$) pair states where S is the total pair spin. The appropriate pair basis functions can be constructed by using

$$|n_aS_a\Gamma_an_b'S_b'\Gamma_b'S\Gamma M\gamma\rangle = \sum_{\substack{M_aM_b'\\ \gamma_a\gamma_b'}} (-1)^{S_a-S_b'+M}(2S+1)^{1/2}[\lambda(\Gamma)]^{1/2} \times \begin{pmatrix} S_a & S_b' & S \\ M_a & M_b' & M \end{pmatrix} V \begin{pmatrix} \Gamma_a & \Gamma_b' & \Gamma \\ \gamma_a & \gamma_b' & \gamma \end{pmatrix} |n_aS_a\Gamma_aM_a\gamma_a\rangle|n_b'S_b'\Gamma_b'M_b'\gamma_b'\rangle \quad (7)$$

where n_a and n_b' label the single-ion configurations involved in the pair state.

In relation to the $M_2X_9^{3-}$ chromophore, the above pair state functions have C_{3v} symmetry, corresponding to the single-ion point group of the pair. When the two single-ion centers are equivalent, one can form symmetric and antisymmetric combinations given by

$$|\pm S_a\Gamma_aS_b'\Gamma_b'S\Gamma M\gamma\rangle = (1/\sqrt{2})[|S_a\Gamma_aS_b'\Gamma_b'S\Gamma M\gamma\rangle \bullet |S_a'\Gamma_a'S_b\Gamma_bS\Gamma M\gamma\rangle] \quad (8)$$

In order to determine the parity correctly, one must use an operator that is capable of distinguishing between these combinations. For D_{3h} pair symmetry, the appropriate operator is σ_h, which is perpendicular to M–M axis. Operating on the pair functions (8) results in

$$\sigma_h|\pm S_a\Gamma_aS_b'\Gamma_b'S\Gamma M\gamma\rangle = (\pm)(-1)^{S_a+S_b'-S+n}(-1)^{\Gamma_a+\Gamma_b'+\Gamma}|\pm S_a\Gamma_aS_b'\Gamma_b'S\Gamma M\gamma\rangle \quad (9)$$

where the (±) sign refers to the symmetric and antisymmetric combinations of C_{3v} bases in (7), and n is the number of electrons. If the function does not change sign on operating with σ_h, it transforms as the appropriate symmetric (Γ') D_{3h} representation; otherwise, it transforms as the antisymmetric (Γ'') representation.

Exchange Interaction. In the case of moderate to strong M–M bonding, the kinetic exchange approximation can be adopted where ferromagnetic contributions involving inter-center electron repulsion terms are neglected.[1] In this case, using the formalism of Tanabe and Fuchikami,[12-14] the effective exchange Hamiltonian can be expressed as

$$H_{ex} = \sum_{\substack{a(\alpha\alpha')\\ b(\beta\beta')}} J(\alpha\alpha',\beta\beta')[-n_a(\alpha\alpha')\, n_b(\beta\beta') - 4S_a(\alpha\alpha')\cdot S_b(\beta\beta') + \delta(\beta\beta')\, n_a(\alpha\alpha') + \delta(\alpha\alpha')\, n_b(\beta\beta')]\, \delta(\alpha\beta')\, \delta(\beta\alpha')/2 \quad (10)$$

where the localized orbitals $\alpha\alpha'$ and $\beta\beta'$ belong to metal centers a and b, respectively, and $\alpha\alpha'$ and $\beta\beta'$ sum over both the t_{2e} and e single-ion orbitals. The generalized occupation number $n(\alpha\alpha')$, spin operator $S(\alpha\alpha')$ and exchange parameter $J(\alpha\alpha',\beta\beta')$ are given by

$$n(\alpha\alpha') = \sum_\sigma a^\dagger_{\alpha\sigma}a_{\alpha'\sigma}$$

$$S(\alpha\alpha') = \sum_{\sigma\sigma'}\langle\sigma|S|\sigma'\rangle a^\dagger_{\alpha\sigma}a_{\alpha'\sigma'}$$

$$J(\alpha\alpha',\beta\beta') = -2h(\alpha\beta')\, h(\beta\alpha')/U \quad (11)$$

where $a_{\alpha\sigma}^\dagger$ and $a_{\alpha\sigma}$ are the familiar creation and annihilation operators operating on spin-orbitals in the second quantization scheme, $h(\alpha\beta)$ is the one-electron transfer or hopping integral, and U is the one-electron transfer energy.

From the real trigonal orbitals given in (2), one can show that

$$h(xx) = h(yy) = (2h_\delta + h_\pi)/3$$

$$h(XX) = h(YY) = (h_\delta + 2h_\pi)/3$$

$$h(xX) = h(yY) = \sqrt{2}(h_\delta - h_\pi)/3 \quad (12)$$

where x and X refer to the t_{2x} and e_x trigonal orbitals, respectively, and h_δ and h_π are related to the cubic orbitals quantized down the C_3^z axis by

$$h_\delta = h(x^2-y^2,x^2-y^2) = h(xy,xy) \qquad h_\pi = h(xz,xz) = h(yz,yz)$$

In the kinetic exchange approximation, the $J(\alpha\alpha',\beta\beta')$ reduce to six unique parameters for the $(t_{2e}^{2-n}e^n)_a(t_{2e}^{2-n}e^n)_b$ pair configuration, which in turn can be expressed in terms of just two exchange parameters, J_π and J_δ, as follows:

$$J(x,x) = (-1/18)[J_\pi + 4J_\delta + 2\sqrt{(J_\pi J_\delta)}]/U$$

$$J(X,X) = (-1/18)[4J_\pi + J_\delta + 2\sqrt{(J_\pi J_\delta)}]/U$$

$$J(x,X) = (-1/9)[J_\pi + J_\delta - 2\sqrt{(J_\pi J_\delta)}]/U$$

$$J(xX,Xx) = (-1/18)[2J_\pi + 2J_\delta + 5\sqrt{(J_\pi J_\delta)}]/U$$

$$J(xx,xX) = (-\sqrt{2}/18)[J_\pi + 2J_\delta - \sqrt{(J_\pi J_\delta)}]/U$$

$$J(xX,XX) = (-\sqrt{2}/18)[2J_\pi + J_\delta + \sqrt{(J_\pi J_\delta)}]/U \quad (13)$$

To be consistent with previous work,[1] we define J_π and J_δ as follows:

$$J_\pi = 4h_\pi^2/U \qquad J_\delta = 4h_\delta^2/U$$

The matrix elements of the various $S(\alpha\alpha')$ and $n(\alpha\alpha')$ operators in H_{ex} can be evaluated by using expressions A1–A3 given in the Appendix. The diagonal energies with respect to H_{ex} are given in Table V. for a number of pair states of interest.

Table V. Diagonal Exchange Energies for Selected Pair States

pair state $\|\pm S_a\Gamma_aS_b\Gamma_bS\Gamma\rangle^a$	multiplet D_{3h} symmetry	diagonal exchange energy[b]
$\|+^3A_2{}^3A_2\ {}^1A_1\rangle$	$^1A_1'$	$3J$
$\|+^3A_2{}^3A_2\ {}^3A_1\rangle$	$^3A_2''$	$2J$
$\|+^3A_2{}^3A_2\ {}^5A_1\rangle$	$^5A_1'$	0
$\|+^3A_2{}^1E\ {}^3E\rangle$	$^3E''$	$2J$
$\|-^3A_2{}^1E\ {}^3E\rangle$	$^3E'$	0
$\|+^3A_2{}^1A_1\ {}^3A_2\rangle$	$^3A_2'$	0
$\|-^3A_2{}^1A_1\ {}^3A_2\rangle$	$^3A_1''$	$2J$
$\|+^1E{}^1E\ {}^1A_1\rangle$	$^1A_1'$	$2J$
$\|+^1E{}^1E\ {}^1A_2\rangle$	$^1A_1''$	$2J$
$\|+^1E{}^1E\ {}^1E\rangle$	$^1E'$	0
$\|+^1E{}^1A_1\ {}^1E\rangle$	$^1E'$	0
$\|-^1E{}^1A_1\ {}^1E\rangle$	$^1E''$	$2J$
$\|+^1A_1{}^1A_1\ {}^1A_1\rangle$	$^1A_1'$	J
$\|+^3A_2{}^3A_2{}^*\ {}^1A_1\rangle$	$^1A_1'$	$2J + 2J' + {}^1/_2J''$
$\|-^3A_2{}^3A_2{}^*\ {}^1A_1\rangle$	$^1A_2''$	$2J + 2J' - {}^1/_2J''$
$\|+^3A_2{}^3A_1{}^*\ {}^1A_2\rangle$	$^1A_2'$	$2J + 2J' + {}^1/_2J''$
$\|-^3A_2{}^3A_1{}^*\ {}^1A_2\rangle$	$^1A_1''$	$2J + 2J' - {}^1/_2J''$
$\|+^3A_2{}^3E^*\ {}^1E\rangle$	$^1E''$	$2J + 2J' - {}^1/_2J''$
$\|-^3A_2{}^3E^*\ {}^1E\rangle$	$^1E'$	$2J + 2J' + {}^1/_2J''$
$\|+^3A_2{}^3A_2{}^\#\ {}^1A_1\rangle$	$^1A_1'$	$3J'$
$\|-^3A_2{}^3A_2{}^\#\ {}^1A_1\rangle$	$^1A_2''$	$3J'$

[a] Single-ion states arising from $t_{2e}^1e^1$ configuration symbolized by *; e^2 configuration symbolized by #, otherwise t_{2e}^2 configuration. [b] Exchange parameters $J = J_{xx}$, $J' = J_{xX}$, and $J'' = J_{xXx}$ can be expressed in terms of J_π and J_δ by using expression 13.

Zeeman Splittings. The Zeeman perturbation for both singly and doubly excited pair states can be written as

$$H_{Zeem} = -(\mu_a + \mu_b)H_z \quad (14)$$

where $\mu_a = -\beta(L_a + 2S_a)$ and similarly for μ_b. It is convenient to use a basis in which the pair spin and orbital moments are coupled according to

$$|\pm S_a\Gamma_aS_b'\Gamma_b'S\Gamma t\tau\rangle = [\lambda(t)]^{1/2}(-1)^{t-\tau}\sum_{M\gamma} V \begin{pmatrix} S & \Gamma & t \\ M & \gamma & -\tau \end{pmatrix} |\pm S_a\Gamma_aS_b'\Gamma_b'S\Gamma m\gamma\rangle \quad (15)$$

where the V coefficient contains spin functions labeled with respect to C_{3v} point group symmetry. For this symmetry, the pair spin functions $|00\rangle$, $|1\pm1\rangle$ and $|10\rangle$ transform as $|A_10\rangle$, $|E\pm1\rangle$ and $|A_20\rangle$, respectively. The $|\pm S_a\Gamma_aS_b'\Gamma_b'S\Gamma M\gamma\rangle$ pair functions in (15) are the same as those given in (8) except for the orbital doublets $|E\tau\rangle$, which contain complex components τ. They are related to the real components via the unitary transformation

$$E_{+1} = (1/\sqrt{2})(-iE_x + E_y) \qquad E_{-1} = (1/\sqrt{2})(iE_x + E_y)$$

(12) Fuchikami, N.; Tanabe, Y. *J. Phys. Soc. Jpn.* **1979**, *47*, 505.
(13) Shigi, H.; Tanabe, Y. *J. Phys. Soc. Jpn.* **1982**, *51*, 1415.
(14) Fuchikami, N.; Block, R. *Physica B+C* **1983**, *119B+C*, 252.

Table VI. Zeeman Splittings for Selected Orbital Doublet Pair States

pair state $\|\pm S_a\Gamma_a S_b\Gamma_b S\Gamma(\Gamma_s)t\tau\rangle^{a,c}$	spin–orbit state D_{3h} symmetry	Zeeman energy (units of βH)^b
$\|+^3A_2{}^3A_2\ {}^3A_1(E)E\pm1\rangle$	$^3A_2''(E')$	$\pm g$
$\|+^3A_2{}^1E\ {}^3E(A_2)E\pm1\rangle$	$^3E''(E'')$	$\pm 2k$
$\|-^3A_2{}^1E\ {}^3E(A_2)E\pm1\rangle$	$^3E'(E')$	$\pm 2k$
$\|+^3A_2{}^1E\ {}^3E(E)E\pm1\rangle$	$^3E''(E')$	$\mp(g + 2k)$
$\|-^3A_2{}^1E\ {}^3E(E)E\pm1\rangle$	$^3E'(E'')$	$\mp(g + 2k)$
$\|+^3A_2{}^1A_1\ {}^3A_2(E)E\pm1\rangle$	$^3A_2'(E'')$	$\pm g$
$\|-^3A_2{}^1A_1\ {}^3A_2(E)E\pm1\rangle$	$^3A_1''(E')$	$\pm g$
$\|+^1E{}^1E\ {}^1E(A_1)E\pm1\rangle$	$^1E'(E')$	$\mp 4k$
$\|+^1E{}^1A_1\ {}^1E(A_1)E\pm1\rangle$	$^1E'(E')$	$\pm 2k$
$\|-^1E{}^1A_1\ {}^1E(A_1)E\pm1\rangle$	$^1E''(E'')$	$\pm 2k$
$\|+^3A_2{}^3E^*\ {}^1E(A_1)E\pm1\rangle$	$^1E''(E'')$	$\pm k'$
$\|-^3A_2{}^3E^*\ {}^1E(A_1)E\pm1\rangle$	$^1E'(E')$	$\pm k'$

$^a\Gamma_s$ is the spin representation in C_{3v} symmetry. $^b g$ is the spin-only g value $\simeq 2$; k and k' are the one-electron orbital-reduction factors defined in (5). ^{c}An asterisk denotes the single-ion state belonging to the $t_{2e}^1e^1$ configuration.

the phases being those of Griffith.[10] From the wave functions given by expression (15) as well as the single-ion orbital moments given in (6), the Zeeman splittings of the pair $|\pm S_a\Gamma_a S_b'\Gamma_b' S\Gamma t\tau\rangle$ spin–orbit basis can be calculated and are listed in Table VI for selected spin–orbit doublet states $|\pm S\Gamma E\tau\rangle$.

Results and Discussion

The preceding sections have laid a theoretical foundation for the analysis of trigonal d^3d^3 M–M σ-bonded dimers. Attention is now turned to a discussion of the main features arising from this theory and their application to the electronic spectra of known pair systems, in particular, $Mo_2X_9^{3-}$ (X = Cl, Br).

Single-Ion States. In the absence of M–M π bonding, the singly excited d^3d^3 pair state energies converge to those calculated for the $t_{2e}^{2-n}e^n$ single-ion configuration in the M–M σ-bond limit. As such, the calculated multiplet energies within the $t_{2e}^{2-n}e^n$ single-ion configuration should serve as a useful starting point in the discussion of the electronic spectra of M–M σ-bonded d^3d^3 dimeric systems.

From the electrostatic energies given in Table IV, the energies of the single-ion $t_{2e}^{2-n}e^n$ multiplets (in units of the Racah B parameter) are plotted in Figure 1 as a function of Δ/B. In this calculation, the Racah C parameter has been set to the value of $4.5B$. For Δ/B values greater than 4, the multiplets group into three distinct levels corresponding to the t_{2e}^2, $t_{2e}^1e^1$, and e^2 configurations in order of increasing energy. The $|t_{2e}^2\ {}^3A_2\rangle$ level remains the ground state for all values of Δ/B but interacts with $|t_{2e}^1e^1\ {}^3A_2\rangle$ as can be seen from Table IV. For moderate to large values of Δ/B, the next two lowest energy multiplets are the spin-forbidden ^1E and $^1A_1$ states belonging to the t_{2e}^2 configuration. Transitions to these two states are expected to be sharp since they have the same Δ/B dependence as the ground state. If configuration interaction is neglected, these two levels lie at $6B + 2C$ and $12B + 4C$, respectively, from the $^3A_2$ ground state (see Table IV). The sharp singly excited pair transitions observed at approximately 8000 and 11 500 cm^{-1} in the electronic spectrum of $Cs_3Mo_2Cl_9$[1] are associated with these two single-ion states in the M–M σ-bond limit.

The next group of multiplets comprise the spin-allowed $^3A_2$, ^3E, and $^3A_1$ states arising from the $t_{2e}^1e^1$ configuration. Transitions from the ground state to the $^3A_2$ and ^3E levels are electric-dipole-allowed and are expected to be broad due to their positive slope as a function of Δ/B with respect to the ground state. Using the ligand field parameters B = 495, C = 1820, and Dq = 1880 cm^{-1} for the $MoCl_6^{3-}$ chromophore, obtained from the recent study of Mo^{3+} doped into the cubic host Cs_2NaYCl_6,[15] the spin-allowed $t_{2e}^1e^1$ multiplets are calculated to lie between 17 500 and 24 000 cm^{-1}. This result is of some significance as broad spin-allowed bands are observed in this region in the electronic spectra of both

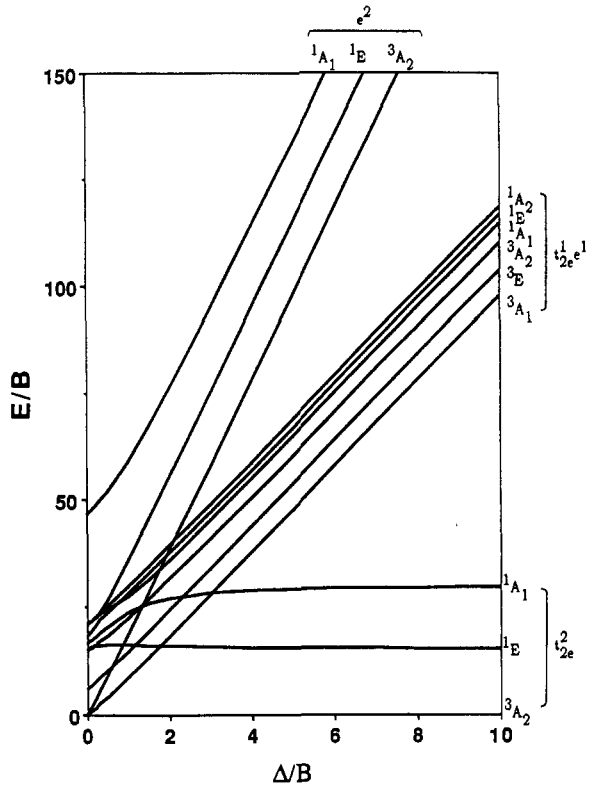

Figure 1. Energies (in units of E/B) of the trigonal $t_{2e}^{2-n}e^n$ single-ion multiplets as a function of Δ/B where Δ is the energy separation of the t_{2e} and e orbitals.

$Mo_2Cl_9^{3-}$ and $Mo_2Br_9^{3-}$.[3-5] The remaining spin-allowed $^3A_2$ state belonging to the e^2 configuration is calculated to lie above 30 000 cm^{-1} and, although electric-dipole-allowed, will most likely be obscured by impurity charge-transfer bands observed in all previous $MoCl_6^{3-}$ and $MoBr_6^{3-}$ spectra between 25 000 and 35 000 cm^{-1}.[4,6,15]

A recent analysis of the 13 000-cm^{-1} absorption band in $Cs_3Mo_2Cl_9$[2] has indicated the presence of a moderate M–M π-exchange interaction, with J_π around 7000 ± 1000 cm^{-1}. Furthermore, as will be shown shortly, a M–M π interaction of this magnitude is indeed necessary to explain the anomalously low orbital g values found for the lower lying multiplets at approximately 8000 cm^{-1}. It is therefore pointless to proceed any further with the analysis of the electronic spectrum of $Mo_2Cl_9^{3-}$ on the basis of the $t_{2e}^{2-n}e^n$ single-ion model alone. In order to model the M–M π interaction correctly, it is necessary to include the full $(t_{2e}^{2-n}e^n)_a(t_{2e}^{2-n}e^n)_b$ pair configuration. From here on J_δ, associated with the M–M δ bonding, will be neglected since recent calculations[16] have shown this overlap to be negligible in $Mo_2Cl_9^{3-}$.

Pair States. The energy levels associated with the $(t_{2e}^{2-n}e^n)_a$-$(t_{2e}^{2-n}e^n)_b$ pair configuration can be calculated by operating on the pair functions (8) with H_{ex} (10). The electrostatic energies given in Table IV must also be included. If configuration interaction is ignored, the diagonal exchange energies of selected pair states (8) are given in Table V. For the $t_{2e}^2t_{2e}^2$ pair configuration, the splitting between (+) and (−) combinations of pair states is seen to be $2J_{xx}$ ($\simeq J\pi/9$) in all cases except for the $^3A_2{}^3A_2$ ground state, whereas for the $(t_{2e}^2)_a(t_{2e}^1e^1)_b$ pair configuration, the splitting is given by J_{xxXx}, which again approximates to $J_\pi/9$. From the value of $J_\pi \simeq$ 7000 cm^{-1} obtained from the analysis of the 13 000-cm^{-1} absorption in $Cs_3Mo_2Cl_9$,[2] first-order exchange splittings of around 800 cm^{-1} are predicted for both the $t_{2e}^2t_{2e}^2$ and $(t_{2e}^2)_a(t_{2e}^1e^1)_b$ pair states shown in Table V.

The energies of selected singly and doubly excited $(t_{2e}^{2-n}e^n)_a$-$(t_{2e}^{2-n}e^n)_b$ pair states are shown in Figure 2 as a function of the M–M π interaction, parametrized by J_π. For this calculation,

(15) Stranger, R.; Moran, G.; Krausz, E.; Güdel, H. U.; Furer, N. *Mol. Phys.* **1990**, *69*, 11.

(16) Stranger, R.; Smith, P. W.; Grey, I. E. *Inorg. Chem.* **1989**, *28*, 1271.

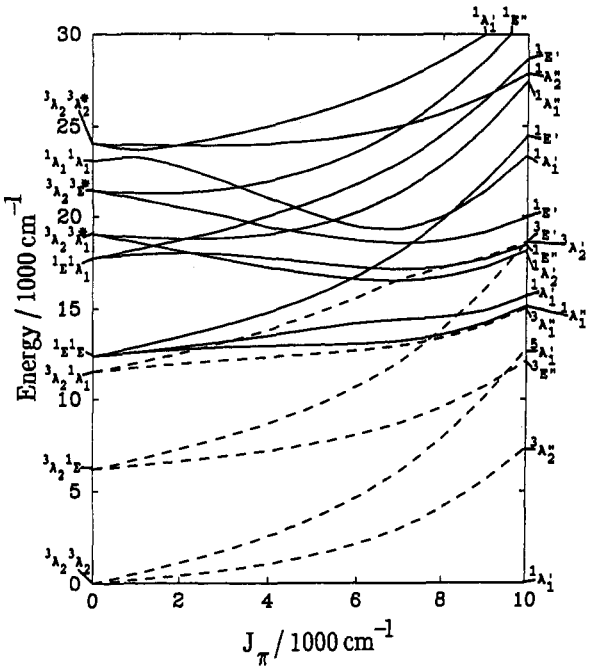

Figure 2. Energies of the $(t_{2e}^{2-n}e^n)_a(t_{2e}^{2-n}e^n)_b$ pair states as a function of J_π, calculated for B = 400 cm^{-1}, C = 4.5B, and Δ = 20 000 cm^{-1}. Only the ground-state S = 0, 1, 2 spin levels, S = 1 singly excited and S = 0 doubly excited pair states belonging to the $t_{2e}^2t_{2e}^2$ configuration, and the S = 0 singly-excited pair states belonging to the $(t_{2e}^2)_a(t_{2e}^1e^1)_b$ configuration are shown. Dashed lines correspond to the S = 1, 2 pair states and full lines to the S = 0 pair states. Pair states are labeled on the lhs of the figure while the resulting D_{3h} multiplets are labeled on the rhs. Pair states arising from the $t_{2e}^1e^1$ single-ion configuration are indicated by an asterisk.

the single-ion ligand field parameters were set at B = 400 cm^{-1}, C = 4.5B and Δ = 20 000 cm^{-1}. The energy levels shown in Figure 2 include only the ground-state S = 0, 1, 2 spin levels, the S = 1 singly excited and S = 0 doubly excited pair states belonging to the $t_{2e}^2t_{2e}^2$ configuration, and the S = 0 singly excited pair states belonging to the $(t_{2e}^2)_a(t_{2e}^1e^1)_b$ configuration.

Overall, for J_π < 5000 cm^{-1}, the energies of pair states belonging to the $t_{2e}^2t_{2e}^2$ configuration are similar to those previously calculated (see Figure 9 of ref 1) by the use of the $t_2^3t_2^3$ model in which the cubic e_g orbitals were neglected. There are differences however. First, the Landē interval separation between the $^1A_1'$, $^3A_2''$ and $^5A_1'$ ground state pair levels breaks down much sooner, in the present case for J_π > 2000 cm^{-1}. Second, in the $t_2^3t_2^3$ model, the splitting between the $^1A_1''$ and $^1A_1'$ doubly-excited pair states increases with J_π. In the present model, this is also occurs until J_π reaches approximately 6000 cm^{-1}, from which the splitting stays relatively constant.

As J_π increases beyond 5000 cm^{-1}, the interaction between pair states belonging to the $t_{2e}^2t_{2e}^2$ and $(t_{2e}^2)_a(t_{2e}^1e^1)_b$ configurations is significant. Eventually, all pair states are factored out to higher energy, mimicking the gradual formation of two M–M π bonds. In the extreme case, where all four electrons are paired off in M–M π bonds, none of the pair states shown in Figure 2 exists, apart from the $^1A_1'$ ground state, and instead, the electronic spectra to low energy will be dominated by MO transitions involving the M–M σ- and π-bonding and antibonding orbitals.

Even with the restricted number of energy levels shown in Figure 2, it is clear that the density of states increases with energy. In particular, a large number of spin-singlet states occur in the 15 000–30 000-cm^{-1} range. Because of the proximity of both singly and doubly excited spin-singlet states in this region, extensive mixing occurs with the likely result of similar transition intensities for both types of states. Clearly, when one or more exchange pathways are significant, extensive configuration interaction can occur. In this case, in order to model the exchange splittings and transition intensities correctly, it is necessary to include the full pair basis set.

Electronic Spectra of $Mo_2X_9^{3-}$ (X = Cl, Br). In relation to previous work, the larger value of $J_\pi \approx$ 7000 cm^{-1} determined from the analysis of the $^1E^1E$ double-excitation region of $Cs_3Mo_2Cl_9$,[2] does not affect the assignments given in ref 1 with the exception of the $^3E'$ level belonging to the singly-excited $^3A_2{}^1E$ pair state. For $J_\pi \approx$ 7000 cm^{-1}1, the ^3E, level is now calculated to lie ≈3000 cm^{-1} to higher energy (see Figure 2), and since no bands were observed below 11 000 cm^{-1}, it seems likely that this level is buried within the singly-excited $^3A_2{}^1A_1$ pair state transition observed at approximately 11 500 cm^{-1}.

Previous work on the spectral region above 16 000 cm^{-1} in $Mo_2Cl_9^{3-}$ has been limited to room-temperature solution or reflectance spectra, where two broads bands were observed at approximately 19 250 and 23 750 cm^{-1}.[3-5] Because of the similarity of the dimer bands above 16 000 cm^{-1} to those of monomeric $MoCl_6^{3-}$, earlier band assignments were in general based on d^3 single-ion transitions from the $^4A_2$ ground state to the spin-allowed $^4T_2$ and $^4T_1$ ligand field states.[4,5] More recently, one-electron transitions within a MO framework have been proposed,[17] but unfortunately, these assignments were based on incorrect polarization data for the lower energy bands.[18]

Since the multiplet structure below 16 000 cm^{-1} has now been successfully assigned on the basis of an exchange-coupled pair, it is more than likely that the spin-allowed bands observed above 16 000 cm^{-1} can also be similarly assigned. Indeed, as seen from Figure 2, a number of spin-allowed pair states associated with the $(t_{2e}^2)_a(t_{2e}^1e^1)_b$ configuration are predicted above 16 000 cm^{-1}, with transitions from the $^1A_1'$ ground state to ^1E, and $^1A_2''$ levels being electric-dipole-allowed. Although these states involve electron occupation of what are formally cubic e_g orbitals, they are only associated with the d^3 $^4T_2$ and $^4T_1$ ligand field states in the weakly coupled limit (J_σ = 0), since M–M σ bonding factors out the trigonal t_{2z} orbitals. The analogous bands in $Mo_2Br_9^{3-}$ have been reported at approximately 18 000 and 22 500 cm^{-1},[4,5] involving a shift of around 1200 cm^{-1} to lower energy in relation to the chloro complex. This shift can be largely attributed to a reduction in Δ for the bromo complex. A detailed magneto-optical study of the spin-allowed bands above 16 000 cm^{-1} in $Cs_3Mo_2Cl_9$ will be reported in a later study.

***g* Values.** The effect of the M–M σ interaction on the g values of the orbitally degenerate d^3d^3 pair states is quite marked. The orbital moments within the $t_2^3t_2^3$ pair configuration can be calculated from the eigenfunctions, obtained from the diagonalization of the pair matrix given in the appendix of ref 1, by using standard group theoretical treatments[10] for the orbital angular momentum operator within the t_2^3 configuration. In the absence of spin–orbit coupling and trigonal field effects, the single-ion ^2E_g state has no orbital moment. However, increasing the value of J_σ results in a progressive mixing of the ^2E and $^2T_{1\pm}$ single-ion states. Since the latter has an orbital moment of 1, the orbital contribution to the singly and doubly excited pair levels involving the ^2E state increases with J_σ. The M–M σ interaction mixes in not only the single excited $^4A_2{}^2T_{1\pm}$ pair state but also the doubly excited $^2E^2T_{10}$ and $^2T_{1\pm}{}^2T_{10}$ pair states. In fact, one can show[19] for large J_σ and J_π = 0, that the $^3E''$ and $^3E'$ multiplets, derived originally from the $^4A_2{}^2E$ pair state, converge to

$$|^3E'\rangle = \tfrac{1}{3}(-\sqrt{2}|^4A_2{}^2E| + 2|^4A_2{}^2T_{1\pm}| + |^2E^2T_{10}| - \sqrt{2}|^2T_{1\pm}{}^2T_{10}|)$$

and

$$|^3E''\rangle = \tfrac{1}{3}(-\sqrt{2}|^4A_2{}^2E| + 2|^4A_2{}^2T_{1\pm}| - |^2E^2T_{10}| + \sqrt{2}|^2T_{1\pm}{}^2T_{10}|)$$

Similarly, the $^1E'$ multiplet, derived originally from the doubly excited $^2E^2E$ pair state, converges to

$$|^1E'\rangle = \tfrac{1}{3}(-|^2E^2E| + 2|^2E^2T_{1\pm}| - 2|^2T_{1\pm}{}^2T_{1\pm}|)$$

(17) Trogler, W. C. *Inorg. Chem.* **1980**, *19*, 697.
(18) Saillant, R.; Wentworth, R. A. D. *Inorg. Chem.* **1969**, *8*, 1226.
(19) Stranger, R. Ph.D. Thesis, University of Tasmania, 1987.

Table VII. Reduced Matrix Elements of $\sum_{\alpha\alpha'}(S\Gamma\gamma\|S(\alpha\alpha')\|S'\Gamma'\gamma')(\alpha\alpha')$ and $\sum_{\alpha\alpha'}(S\Gamma\gamma\|n(\alpha\alpha')\|S\Gamma'\gamma')(\alpha\alpha')$[a]

	$^3A_2$	$^1A_1$	^1E_x	^1E_y	$^3A_2$*	$^3A_1$*	^3E_x*	^3E_y*
$^3A_2$	$xx + yy$	$xy - yx$	$xy + yx$	$xx - yy$	$xX + yY$	$-xY + yX$	$-xY - yX$	$-xX + yY$
$^1A_1$		$xx + yy$	$-xx + yy$	$xy + yx$	$-xY + yX$	$-xX - yY$	$xX - yY$	$-xY - yX$
^1E_x			$xx + yy$	$-xy + yx$	$xY + yX$	$xX - yY$	$-xX - yY$	$xY - yX$
^1E_y				$xx + yy$	$xX - yY$	$-xY - yX$	$-xY + yX$	$-xX - yY$
$^3A_2$*					$xx + yy + XX + YY$	$xy - yx - XY + YX$	$xy + yx - XY - YX$	$xx - yy - XX + YY$
$^3A_1$*						$xx + yy + XX + YY$	$-xx + yy - XX + YY$	$xy + yx + XY + YX$
^3E_x*							$xx + yy + XX + YY$	$-xy + yx - XY + YX$
^3E_y*								$xx + yy + XX + YY$

	$^1A_2$*	$^1A_1$*	^1E_x*	^1E_y*	$^3A_2$#	$^1A_1$#	^1E_x#	^1E_y#
$^3A_2$	$-xX - yY$	$xY - yX$	$xX + yY$	$xX - yY$				
$^1A_1$	$xY - yX$	$xX + yY$	$-xX + yY$	$xY + yX$				
^1E_x	$-xY - yX$	$-xX + yY$	$xX + yY$	$-xY + yX$				
^1E_y	$-xX + yY$	$xY + yX$	$xY - yX$	$xX + yY$				
$^3A_2$*	$xx + yy - XX - YY$	$xy - yx + XY - YX$	$xy + yx + XY + YX$	$xx - yy + XX - YY$	$xX + yY$	$xY - yX$	$xY + yX$	$xX - yY$
$^3A_1$*	$-xy + yx - XY + YX$	$xx + yy - XX - YY$	$-xx + yy - XX - YY$	$xy + yx + XY - YX$	$-xY + yX$	$xX + yY$	$-xX + yY$	$xY + yX$
^3E_x*	$xy + yx + XY + YX$	$-xx + yy + XX - YY$	$xx + yy - XX - YY$	$-xy + yx + XY - YX$	$xY + yX$	$-xX + yY$	$xX + yY$	$-xY + yX$
^3E_y*	$xx - yy + XX - YY$	$xy + yx - XY - YX$	$xy - yx - XY + YX$	$xx + yy - XX - YY$	$xX - yY$	$xY + yX$	$xY - yX$	$xX + yY$

	$^1A_2$*	$^1A_1$*	^1E_x*	^1E_y*	$^3A_2$#	$^1A_1$#	^1E_x#	^1E_y#
$^1A_2$*	$xx + yy + XX + YY$	$xy - yx - XY - YX$	$xy + yx - XY - YX$	$xx - yy - XX + YY$	$xX + yY$	$xY - yX$	$xY + yX$	$xX - yY$
$^1A_1$*		$xx + yy + XX + YY$	$-xx + yy - XX + YY$	$xy + yx + XY + YX$	$-xY + yX$	$xX + yY$	$-xX + yY$	$xY + yX$
^1E_x*			$xx + yy + XX + YY$	$-xy + yx - XY + YX$	$xY + yX$	$-xX + yY$	$xX + yY$	$-xY + yX$
^1E_y*				$xx + yy + XX + YY$	$xX - yY$	$xY + yX$	$xY - yX$	$xX + yY$
$^3A_2$#					$XX + YY$	$XY - YX$	$XY + YX$	$XX - YY$
$^1A_1$#						$XX + YY$	$-XX + YY$	$XY + YX$
^1E_x#							$XX + YY$	$-XY + YX$
^1E_y#								$XX + YY$

[a] An asterisk denotes a state belonging to the $t_{2e}^1e^1$ single-ion configuration. [b] A # denotes state belonging to the e^2 single-ion configuration.

The dependence of orbital moments on J_σ for the singly excited $^4A_2{}^2E$ and doubly excited $^2E^2E$ pair states is shown in Figure 3. Clearly, for $J_\sigma > 2000$ cm^{-1}, the orbital moments have converged to the values $2k$ and $4k$, respectively.

The mixing of the ^2E and $^2T_{1\pm}$ single-ion states by J_σ has been recently observed in the trigonal Cr^{3+} pair tris(μ-hydroxy)bis-(1,4,7-trimethyl-1,4,7-triazacyclononane)chromium(III),[20] where the axial M–M exchange is much weaker with $J_\sigma \approx 2200$ cm^{-1}. From Figure 3, an orbital moment of approximately 2 (for $k = 1$) is predicted for the singly excited $^4A_2{}^2E$ pair state in excellent agreement with the reported values between 1.95 and 2.05 for this complex.

From the recent magneto-optical study of $Cs_3Mo_2Cl_9$,[1] the orbital moments for the singly excited $^3A_2{}^1E$ pair state (associated with the $^4A_2{}^2E$ state in the weakly coupled limit) were found to lie in the range 0.5–0.8. These values deviate significantly from the predicted value of 2 (for $k = 1$), yet J_σ is approximately 20000 cm^{-1}, 10 times greater than that found for the tris(μ-hydroxy) Cr^{3+} pair. Apart from J_σ, an obvious difference between the two pair systems is the magnitude of J_π. For the Cr^{3+} complex, J_π is quite small, approximately 180 cm^{-1}, whereas for the Mo^{3+} pair, the analysis of the $^1E.{}^1E$ double excitation has indicated $J_\pi \simeq 7000$ cm^{-1}.

Within the $t_2^3t_2^3$ exchange-coupled pair model, inclusion of J_π makes a negligible difference in the calculated orbital moments. This is not the case for the $(t_{2e}^{2-n}e^n)_a(t_{2e}^{2-n}e^n)_b$ pair configuration where the cubic e_g orbitals are included. For this configuration, increasing J_π causes extensive mixing between the t_{2e} and e single-ion orbitals, and this leads to a dramatic departure from the orbital moments and Zeeman splittings (see Table VI) predicted for certain of the $t_{2e}^2t_{2e}^2$ pair states.

Orbital moments can be calculated from eq 6 and the eigenfunctions obtained from the diagonalization of the complete $(t_{2e}^{2-n}e^n)_a(t_{2e}^{2-n}e^n)_b$ pair configuration. The effect of increasing J_π on the orbital moments for the $^3E'$ and $^3E''$ multiplets belonging to the singly excited $^3A_2{}^1E$ pair state is shown in Figure 4. In the absence of any M–M π bonding ($J_\pi = 0$), the orbital moments for the $t_{2e}^2t_{2e}^2$ pair states correspond to those calculated for the $t_2^3t_2^3$ pair configuration in the M–M σ-bonded limit, in particular, values of $2.0k$ and $4.0k$ are calculated for the singly excited $^3A_2{}^1E$ and doubly excited $^1E^1E$ pair states, respectively (see Table VI). If the single-ion e_g orbitals are included in the calculation, slightly lower values are obtained, as seen from Figure 4, due to the mixing of t_{2e}^2 and $t_{2e}^1e^1$ single-ion states by the electrostatic interaction. As J_π increases, the orbital moment for the $^3E'$ multiplet remains relatively stable at approximately $2k$. In contrast, the orbital moment for the $^3E''$ multiplet decreases dramatically from $\simeq 2k$ at $J_\pi = 0$, to $1.0k$ and $0.5k$ for $J_\pi = 8000$ and 12000 cm^{-1}, respectively. The latter values are in good agreement with those observed experimentally, especially for $k < 1$, and confirm the presence of a moderate M–M π-exchange interaction ($J_\pi \simeq 7000$ cm^{-1}), in the $Cs_3Mo_2Cl_9$ exchange-coupled pair.

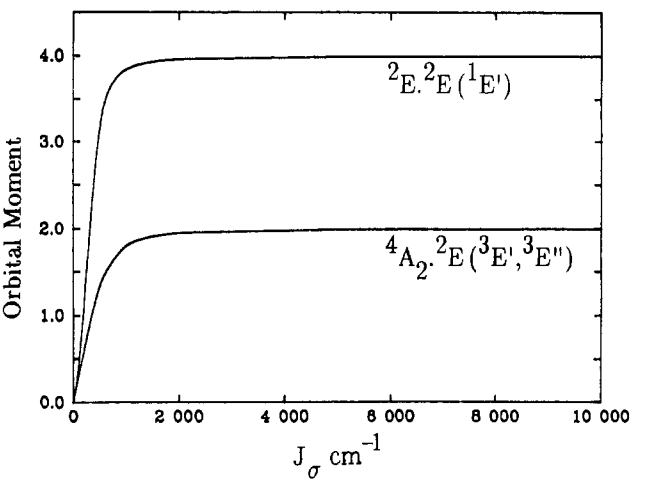

Figure 3. Dependence on J_σ of the orbital moments for the $^4A_2{}^2E$ and $^2E^2E$ pair states using the $t_2^3t_2^3$ exchange-coupled model of ref 1. Calculation was performed for $B = 467$ cm^{-1}, $C = 4B$, and $Dq = 1920$ cm^{-1}.

Metal–Metal Bonding. The value of $J_\pi \approx 7000$ cm^{-1} found from the analysis of the $^1E^1E$ double excitation,[2] as well as the present study, is now in far better agreement with observed J_π/J_σ ratios between 0.1 and 0.3 for other trigonal d^3d^3 dimers.[20,21] Furthermore, it compares well with $J_\pi/J_\sigma \approx 0.3$ determined from

(20) Riesen, H.; Güdel, H. U. *Mol. Phys.* **1987**, *60*, 1221.

(21) Riesen, H.; Güdel, H. U. *Inorg. Chem.* **1984**, *23*, 1880.

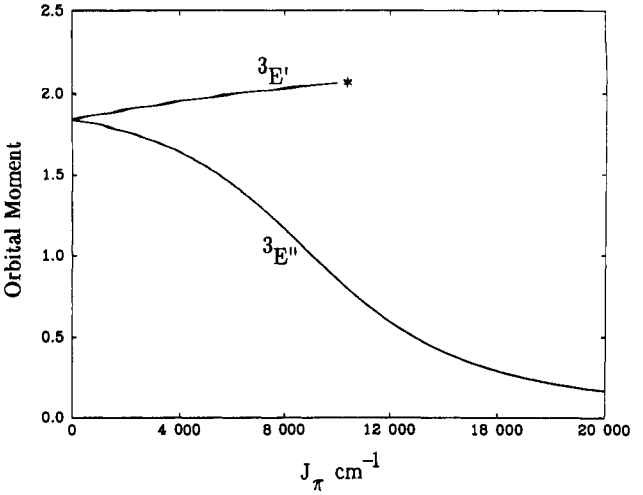

Figure 4. Dependence on J_π of the orbital moments for the $^3E'$ and $^3E''$ multiplets of the singly excited $^3A_2{}^1E$ pair state. Calculation was performed for $B = 400$ cm^{-1}, $C = 4.5B$, and $\Delta = 20\,000$ cm^{-1}. An asterisk denotes that the curve for the $^3E'$ multiplet is shown only to $J_\pi = 10\,000$ cm^{-1}, as discrimination from other $^3E'$ multiplets is not possible beyond this range.

Table VIII. Coefficients for the Reduced Matrix Elements of $S(\alpha\alpha')$ and $n(\alpha\alpha')$ Given in Table VII[a]

n	n'	S	S'	$S(\alpha\alpha')$	$n(\alpha\alpha')$
0	0	1	1	$\sqrt{3}/\sqrt{2}$	1
0	0	0	0	0	1
0	0	0	1	$-\sqrt{3}/2$	0
0	1	1	1	$\sqrt{3}/2$	$1/\sqrt{2}$
0	1	0	0	0	$1/\sqrt{2}$
0	1	0	1	$-\sqrt{3}/2\sqrt{2}$	0
0	2	1	1	$\sqrt{3}/\sqrt{2}$	1
0	2	0	0	0	1
0	2	0	1	$-\sqrt{3}/2$	0
1	1	1	1	$\sqrt{3}/2\sqrt{2}$	1/2
1	1	0	0	0	1/2
1	1	0	1	$-\sqrt{3}/4$	0
1	2	1	1	$\sqrt{3}/2$	$1/\sqrt{2}$
1	2	0	0	0	$1/\sqrt{2}$
1	2	0	1	$-\sqrt{3}/2\sqrt{2}$	0
2	2	1	1	$\sqrt{3}/\sqrt{2}$	1
2	2	0	0	0	1
2	2	0	1	$-\sqrt{3}/2$	0

[a] n and n' label the single-ion configurations involved in the reduced matrix element where $t_{2e}^2 = 0$, $t_{2e}^1e^1 = 1$, and $e^2 = 2$. Coefficient remains unchanged when n and n' and/or S and S' are interchanged.

extended Huckel calculations[20,22] on the analogous Cr^{3+}, V^{2+}, V^{3+}, and Ti^{3+} dimers.

Although J_π is nearly 30% of the value of J_σ, the effect on the M–M π-bonding–antibonding e′–e″ molecular orbital separation (see Figure 2 of ref 17) is considerably smaller. This difference arises because J_π is defined in terms of cubic orbitals quantized down the trigonal axis, whereas the e′ and e″ molecular orbitals are by necessity defined in terms of trigonally adapted metal t_{2g} orbitals. The transformation between these orbital bases and associated exchange parameters is given by (2) and (13), respectively, with the result that the increase in the e′–e″ separation is only $^1/_{18}$th of the increase in J_π. As such, within the molecular orbital framework, the M–M π-bonding interaction is still quite weak, being only about 3% of the M–M σ interaction.

Appendix

The matrix elements involving the operators $S(\alpha\alpha')$ and $n(\alpha\alpha')$ in H_{ex} (eq 10) can be evaluated from

$$\langle n_aS_a\Gamma_an_bS_b\Gamma_bS\Gamma M\gamma|S_a(\alpha\alpha')\cdot S_b(\beta\beta')|n_a'S_a'\Gamma a'n_b'S_b'\Gamma_b'S\Gamma'M'\gamma'\rangle = \sum_{\substack{\gamma_a\gamma_a'\\ \gamma_b\gamma_b'}} \delta(SS')\,\delta(MM')\,[\lambda(\Gamma)]^{1/2}[\lambda(\Gamma')]^{1/2}(-1)^{S_a'+S_b+S} \times V\begin{pmatrix}\Gamma_a & \Gamma_b & \Gamma\\ \gamma_a & \gamma_b & \gamma\end{pmatrix}V\begin{pmatrix}\Gamma_a' & \Gamma_b' & \Gamma'\\ \gamma_a' & \gamma_b' & \gamma\end{pmatrix}\begin{Bmatrix}S_a & S_b & S\\ S_b' & S_a' & 1\end{Bmatrix} \times \langle n_aS_a\Gamma_a\gamma_a||S_a(\alpha\alpha')||n_a'S_a'\Gamma_a'\gamma_a'\rangle\langle n_bS_b\Gamma_b\gamma_b||S_b(\beta\beta')||n_b'S_b'\Gamma_b'\gamma_b'\rangle \quad (A1)$$

$$\langle n_aS_a\Gamma_an_bS_b\Gamma_bS\Gamma M\gamma|n_a(\alpha\alpha')\ n_b(\beta\beta')|n_a'S_a'\Gamma_a'n_b'S_b'\Gamma_b'S\Gamma'M'\gamma'\rangle = \sum_{\substack{\gamma_a\gamma_a'\\ \gamma_b\gamma_b'}} \delta(S_aS_a')\,\delta(S_bS_b')\,\delta(SS')\,\delta(MM') \times [\lambda(\Gamma)]^{1/2}[\lambda(\Gamma')]^{1/2}(-1)^{S_a'+S_b+S} \times V\begin{pmatrix}\Gamma_a & \Gamma_b & \Gamma\\ \gamma_a & \gamma_b & \gamma\end{pmatrix}V\begin{pmatrix}\Gamma_a' & \Gamma_b' & \Gamma'\\ \gamma_a' & \gamma_b' & \gamma\end{pmatrix} \times \langle n_aS_a\Gamma_a\gamma_a||n_a(\alpha\alpha')||n_a'S_a'\Gamma_a'\gamma_a'\rangle\langle n_bS_b\Gamma_b\gamma_b||n_b(\beta\beta')||n_b'S_b'\Gamma_b'\gamma_b'\rangle \quad (A2)$$

$$\langle n_aS_a\Gamma_an_bS_b\Gamma_bS\Gamma M\gamma|n_a(\alpha\alpha')|n_a'S_a'\Gamma_a'n_b'S_b'\Gamma'M'\gamma'\rangle = \sum_{\substack{\gamma_a\gamma_a'\\ \gamma_b\gamma_b'}} \delta(n_bn_b')\,\delta(S_aS_a')\,\delta(S_bS_b')\,\delta(\Gamma_b\Gamma_b')\,\delta(\gamma_b\gamma_b')\,\delta(SS') \times \delta(MM')\,[\lambda(\Gamma)]^{1/2}[\lambda(\Gamma')]^{1/2}\langle n_aS_a\Gamma_a\gamma_a||n_a(\alpha\alpha')||n_a'S_a'\Gamma_a'\gamma_a'\rangle \quad (A3)$$

where in this case the V coefficient corresponds to Griffith's real trigonal basis,[10] and n_a and n_b label the single-ion configurations involved in the pair states. The reduced matrix elements of the operators $\sum_{\alpha\alpha'}S(\alpha\alpha')$ and $\sum_{\alpha\alpha'}n(\alpha\alpha')$ over the multiplets arising in the $t_{2e}^{2-n}e^n$ single-ion configuration can be determined from Table VII by multiplying by the appropriate coefficient given in Table VIII. Furthermore, the relations

$$\langle S'\Gamma'\gamma'||S(\alpha\alpha')||S\Gamma\gamma\rangle = (-1)^{S-S'}\langle S\Gamma\gamma||S(\alpha'\alpha)||S'\Gamma'\gamma'\rangle$$

$$\langle S\Gamma'\gamma'||n(\alpha\alpha')||S\Gamma\gamma\rangle = \langle S\Gamma\gamma||n(\alpha'\alpha)||S\Gamma'\gamma'\rangle \quad (A4)$$

also apply.

(22) Leuenberger, B.; Güdel, H. U. *Inorg. Chem.* **1986**, *25*, 181.

Registry No. $Mo_2Cl_9^{3-}$, 52409-23-1; $Mo_2Br_9^{3-}$, 45976-45-2.